UNIVERSITY OF MISKOLC
FACULTY OF MECHANICAL ENGINEERING AND INFORMATICS

DETECTION OF THE DAMAGES OF COMPOSITE MACHINE AND VEHICLE STRUCTURES WITH ACOUSTIC METHODS

Booklet of PhD Theses

PREPARED BY:

SAAD JABBER NAZAL ALSARAYEFI

Engineering of Mechanics … (BSc),
Engineering of Mechanics/ Design … (MSc)

ISTVÁN SÁLYI DOCTORAL SCHOOL OF MECHANICAL ENGINEERING SCIENCES
TOPIC FIELD OF MECHANICAL ENGINEERING SCIENCES
TOPIC GROUP OF DESIGN OF MACHINES AND ELEMENTS

HEAD OF DOCTORAL SCHOOL

Dr. Gabriella Bognár Vadászné
DSc, Full Professor

Head of Topic Group

Dr. Gabriella Bognár Vadászné
DSc, Full Professor

Scientific Supervisor

Dr. Gabriella Bognár Vadászné
DSc, Full Professor
Dr. Károly Jálics
PhD, Associate Professor

Miskolc
2022

JUDGING COMMITTEE

chair:

secretary:

members:

OFFICIAL REVIEWERS

1. INTRODUCTION

1.1. Motivation

Composite materials usages have been remarkably increased in almost all industry sectors. Fibre reinforced polymer (FRP) composites in particular, are significantly adopted in aerospace and automobile structures to satisfy the need for materials that are light in weight, costly effective, and good impact absorbents [1]. Generally, the most important properties of FRP composites that making them attractive to industries sectors are high specific strength, high specific stiffness, high fracture resistance, good abrasion, corrosion, impact, and fatigue resistance, and low cost [2].

On the other hand, damages may arise in the FRP components during operation putting the structure in a risk [3]. Due to the heterogeneous microstructure of the materials and big difference of the constituent's properties, the mechanism of the damage is not smoothly predicted and understood. Also, the interface presence and the fibre orientations give anisotropy in overall properties of the materials [4].

FRP components can show damages that are not visible after impact, crash. The component that is not visibly damaged loses its load capacity or its original energy absorption capacity. This can lead to undefined component failure during further load. A recorded failure history can provide important information concerning a possible propagation of damages to complete failure. Damaged FRP components can be detected and replaced by means of damage detection methods. Costs can be reduced, because components no longer have to be replaced as a precautionary measure [5].

In order to have an early prediction of existence of visible or non-visible damages in composite structure and avoid failure, many structural health monitoring (SHM) methods have been revealed. Among these methods are guided waves method, acoustic emission methods, wave field imaging, modal analysis, frequency response function method, and others. Thus, a lot of attention has been paid to the issue of damages detection in composite materials structures using acoustic emission and vibration-based methods [6].

1.2. Objectives

The global aim of this reserach work is to the identification and tracking of visible and non-visible damage (delamination, fibre and matrix fractures) due to a test bench load using online and/or offline acoustic based measurements. Specifically:

i. Using the SHM methods that are based on vibrational responce of the material to track the defects or damages of the composite materials. Modal analysis, Vibration decay rate, and accoustic emission are the methods used in the current work.

ii. These methods can show parameters such as the modal frequencies and mode shapes which are very effctive to study characteristics of a structure in case of damaged or non-damaged and the measured data shows an estimation of the dynamic behaviour of the target part.
iii. Investigating the damping response offered by a damaged/undamaged fibre reinforced polymer plate and compare between the two cases in order to have as much information as possible about composite structure conditions.
iv. To determine the modal behaviour of the used specimen under different preload condition.
v. To highlight the ability and sensitivity of the above methods for detecting damages in composite materials.

2. METHODOLOGY

The first part of my dissertation work includes theoretical study on the material that will be the specimen for the laboratory work. Namely, Glass fiber reinforced polymer (GFRP) material is used as specimen with definite dimensions to do our tests. In addition, there are experimental investigations done to detect damage of the composite specimen by using the vibrational based methods and to find whether the methods used are sensitive or not to damage existence in the composite specimen. All the investigations are discussed in the following sections.

2.1 Optimum Fiber Size for a Fiber Glass – Epoxy Composite

This work studies the relationship between the fiber diameter (optimum) and the longitudinal tensile strength when designing materials based on representative volume element (RVE) or a unit cell, using an optimisation algorithm.

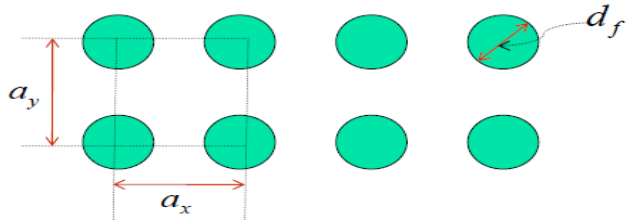

Figure 1. Square Unit Cell with Four-Fiber Arrangement [6].

Swarm intelligence optimisation algorithms are used to estimate the optimal size of the glass fiber of circular cross-section of a glass-epoxy composite. Finding the best fiber size in a composite material has significant benefits on cost reduction. A comparative study was done to select optimal fiber diameter that can satisfy the optimal longitudinal tensile strength. Particle Swarm Optimisation algorithm (PSO) and artificial bee colony algorithm ABC are proposed for this comparative study.

Depending on the possible periodic distribution of the fibre in the composite materials, the RVE or unit cell might be of square or hexagonal packing array. In the theory of composite materials, the unit cell is modelled based on assumption such as the homogeneity of the composite material. Taking into consideration the square unit cell with four fibre arrangement (Figure 1), the longitudinal tensile strength can be calculated using the equation:

$$F_{1t} = F_{ft}\left(v_f + \frac{E_m}{E_f}\right)(1 - v_f) \tag{1}$$

where:

F_{1t}: *Longitudinal Tensile Strength*

F_{ft}: *Fiber Tensile Strength*

v_f: *Fiber Volume Fraction*

E_m: *Matrix Young's Modulus*

E_f: *Fiber Young's Modulus*

And since Since the volume fraction of the fiber is given by:

$$vf = \frac{\text{volume of the fiber}}{\text{total volume}} = \frac{\frac{\pi}{4}(df)^2}{ax.ay} \tag{2}$$

A direct relationship exists between the fibre and the longitudinal tensile strength.

2.1.1 Optimization Algorithm

Particle swarm optimisation PSO is a powerful and efficient optimisation algorithm which is widely used for a wide range of applications. PSO mimics the swarm behaviour of fish and birds, we can call the members of the swarm and the swarm itself as particles and population respectively, and every agent is a candidate solution to the optimisation problem. The position and velocity of a specific particle is denoted by:

$x_k(t) \in x$

$v_k(t) \in x$

Where k is the index of the agent in the swarm and x is the search area while (t) is the iteration number of the algorithm. The standard PSO is as follows

$$x_{kj}(t+1) = x_{kj}(t) + v_{kj}(t+1) \tag{3}$$

$$v_{kj}(t+1) = w * v_{kj}(t) + r_1 C_1(p_{kj}(t) - x_{kj}(t)) + r_2 C_2(G_j(t) - x_{kj}(t)) \tag{4}$$

- $v_{kj}(t+1)$: denote the velocity of particle k in time step (t+1) and the jth component for this velocity
- r_1, r_2 : a random number in the range 0 to 1
- C_1,C_2 : acceleration coefficient
- w: inertia coefficient
- $w * v_{kj}(t)$: inertia term
- $r_1 C_1(p_{kj}(t) - x_{kj}(t))$: cognitive component
- $r_2 C_2(G_j(t) - x_{kj}(t))$: social component
- Equations (1) and (.2) are the main rules that PSO employ for the search process.

2.1.2 Optimization Algorithm

Strength problem is a maximisation optimisation problem which depends on six main parameters, and the whole issue can be described as follow:

Consider

$$\vec{x} = [x_1 \quad x_2 \quad x_3 \quad x_4 \quad x_5 \quad x_6] = [d \quad a_x \quad a_y \quad E_m \quad F_{ft} \quad E_f]$$

Maximise

$$f(\vec{x}) = f_{1t} = F_{ft}\left(v_f + \frac{E_m}{E_f}\right)(1 - v_f) \tag{5}$$

Subject to:

- $v_f \leq 0.6$
- $F_{1t} \leq 2.5\ GPa$
- $5 * 10^{-6} \leq d \leq 40 * 10^{-6}$
- $50 * 10^{-6} \leq a_x \leq 100 * 10^{-6}$
- $50 * 10^{-6} \leq a_y \leq 100 * 10^{-6}$
- $2 * 10^9 \leq E_m \leq 5 * 10^9$
- $2 * 10^9 \leq F_{ft} \leq 5 * 10^9$
- $40 * 10^9 \leq E_f \leq 80 * 10^9$

The above-mentioned constraints were chosen based on characteristics of the fiber and epoxy considering the minimum and maximum values (from literature). Figure 2 shows the performance of PSO on this constrained optimisation problem where it is required to find the best possible set of variables that can meet the requirement of the constraints. It is worth to mention that for the set of variables in table 1, the corresponding maximum F_{ft} is 2.8241e+09 while v_f is 0.5027. Figure 2 shows the PSO algorithm on the maximum strength equation.

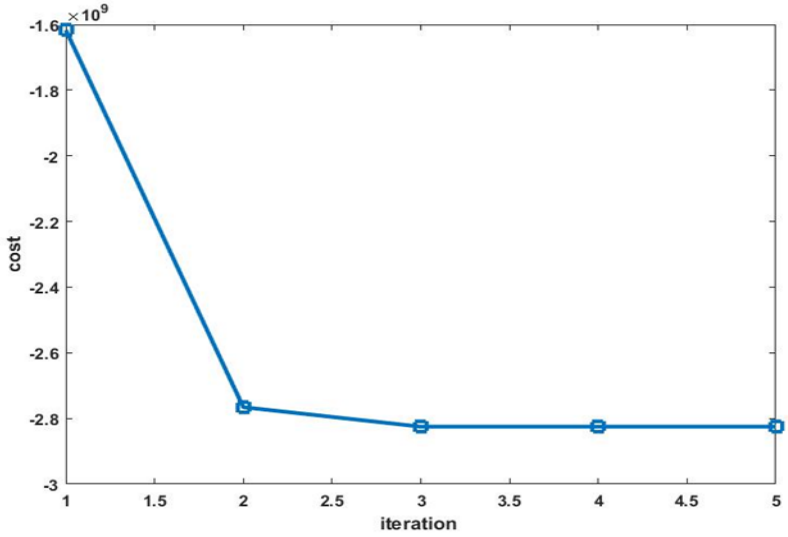

Figure 2. *The Convergence of the PSO on Maximum Strength Equation.*

Table 1. Best Possible Results for the Constrained Problem.

Parameter	***d mm***	***ax mm***	***ay mm***	***Em. GPa***	***Fft. GPa***	***Ef. GPa***
Value	4.0e-05	5.0e-05	5.0e-05	5	5	40

2.2 Micromechanical Analysis of Glass Fiber/Epoxy Lamina

Current work deals with the evaluation of the engineering constants such as longitudinal young modulus E_1, transverse young modulus E_2, in plane shear modulus G_{12}, and Poisson ratio V_{12} of unidirectional fiber reinforced composite. These properties are calculated by theory of elasticity based on a representative volume element (RVE) or a unit cell [7]. The methods used are the rule of mixture (ROM, Halphin-Tsai, cylindrical assemblage model (CAM), and periodic microstructure model (PMM). A square unit cell was adopted to carry out the micromechanics calculation in this work [8].

Current work investigates the mechanical behavior of a unidirectional fiber reinforced polymer composite lamina consisting of fibers embedded in epoxy resin as a matrix. Micromechanical analysis is done on a square-patterned unit cell of the above composite to predict the longitudinal modulus (E_1), Transverse modulus (E_2), In-plane shear modulus (G_{12})

and Major Poisson's ratio (ν_{12}). These engineering constants are evaluated to three types of fiber (E-Glass, R-Glass, and S- Glass) with various fiber volume fraction based on theory of elasticity approach. Computer Aided Design Environment for Composites (CADEC) software is used to do the numerical analysis. This theoretical investigation helps to realize the bearing ability of unidirectional fiber reinforced composite subjected to longitudinal load by analyzing the engineering design constants.

The focus of current work is to evaluate the engineering properties of a fiber reinforced composite material of a unidirectional fiber based on square array of RVE. The analysis is done using analytical methods such as rule of mixture, Halphin-Tsai, cylindrical assemblage model CAM, and periodic microstructure model PMM. These methods were used individually to calculate modulus in the direction of the fibers E_1, modulus in the transverse-to-fiber direction E_2, In-plane shear modulus G_{12}, and In-plane Poisson's ratio ν_{12}. All calculations are done based on the assumption that the material is anisotropic and homogenous and all formulas are applied to a unit cell. The study is carried out on three types of materials which are E-galss/Epoxy, S-glass/Epoxy, and R-glass/Epoxy with different fiber volume fraction Vf, and the results are compared and analysed.

2.2.1 Rule of Mixture

For a unit cell, the longitudinal modulus:

$$E_1 = E_f V_f + E_m V_m \tag{6}$$

Poisson's ratio:

$$\nu_{12} = \nu_f V_f + \nu_m V_m \tag{7}$$

where:

E_f: Fiber elastic modulus
V_f: Fiber volume fraction
E_m: Matrix elastic modulus
Vm: Matrix volume fraction
ν_f : Fiber Poisson's ratio
ν_m : Matrix Poisson's ratio
ν_{12}: Poisson's ratio for plane 1-2

2.2.2 Inverse Rule of Mixture

The modulus that is perpendicular to fiber direction (Transverse Modulus) E_2:

$$\frac{1}{E_2} = \frac{V_m}{E_m} + \frac{V_f}{E_f} \tag{8}$$

2.2.3 Halpin-Tsai Equation

The results of this equation are more accurate and beneficial for analytical evaluation and design purposes.

$$E_2 = E_m \left[\frac{1+\zeta \eta V_f}{1-\eta E_f}\right] \quad (9)$$

where:

$$\eta = \frac{\frac{E_f}{E_m}-1}{\frac{E_f}{E_m}+\zeta}$$

$\zeta = 2$ for circular and square fiber, $\zeta = 2\frac{a}{b}$ for rectangular fiber

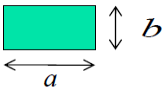

2.2.4 Cylindrical Assemblage Model (CAM) Formula

Shear Modulus in the 1-2 Planes G_{12}:

$$G_{12} = G_m \left[1 + \frac{V_f\left(1-\frac{G_m}{G_f}\right)}{\frac{G_m}{G_f}+S_3\left(1-\frac{G_m}{G_f}\right)}\right] \quad (10)$$

where: G_m: Matrix Shear Modulus

G_f: Fiber shear modulus

2.2.5 Periodic Micro-Structure Model (PMM) Formula

$$G_{12} = G_m \left[1 + \frac{V_f\left(1-\frac{G_m}{G_f}\right)}{\frac{G_m}{G_f}+S_3\left(1-\frac{G_m}{G_f}\right)}\right] \quad (11)$$

where: $S_3 = 0.49 - 0.47V_f - 0.027\,V_f^2$ [9].

2.2.6 Results

For all suggested volume fractions v_f, the longitudinal young's modulus E_1 of the E-glass / Epoxy is lower than those of R-glass / Epoxy and S-glass / Epoxy which they seemed to have very close young's modulus all over the variation of v_f.

The longitudinal young's modulus E_1 increases linearly with increase in fiber volume fraction for all the three types of composites materials proving the fact that the strength of the unidirectional fiber composite is as high as the fiber volume fraction high since the fiber is stiffer and stronger see figure 3.

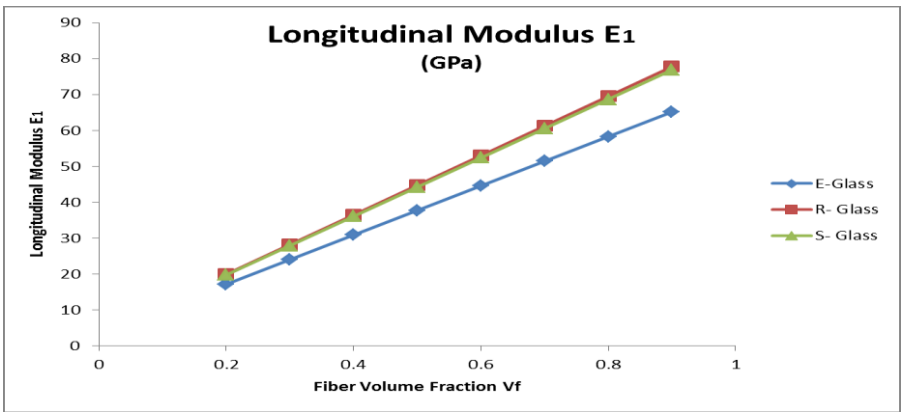

Figure 3. Variation of E_1 with Fiber Volume Fraction for all Fibers.

As shown in the Figures (4-12) below, that for each material the transverse modulus E_2 is calculated in two ways, rule of mixture ROM and Halphin-Tsai. The in-plane shear modulus G_{12} is evaluated by the cylindrical assemblage model CAM and the periodic microstructure model PMM. The in-plane Poisson's ratio for each type of materials is calculated based on the ROM and PMM. Comparison is made between each two different results of each constant. Furthermore, variation of longitudinal young modulus with the volume fraction for all types of composite materials is done. From above graphs, some findings can be stated:

- The transverse young's modulus E_2 increases linearly with increase in fiber volume fraction for all the three types of composites materials up to 80 % of volume fraction and rapid increase happens after that.
- For all three types of materials, the magnitude of E_2 computed by ROM is much lower than this computed by Halphin-Tsai methods for all fiber volume fractions, pulling to the mind the fact that the ROM equation under-estimates the actual value for E_2 while the Halphin-Tsai methods gives more accurate results of it
- In plane shear modulus G_{12} increases linearly with increase in fiber volume fraction for all the three types of composites materials, but, after 80% of the Vf, there is noticeable difference of G_{12} computed by CAM and PMM methods.

(E-Glass / Epoxy lamina)

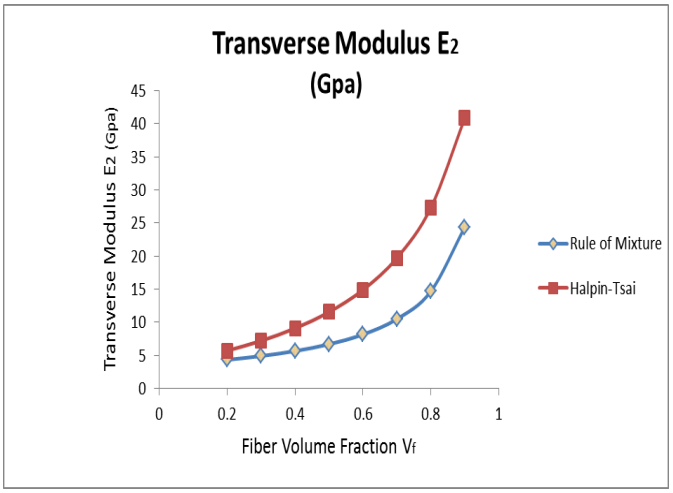

Figure 4. Variation of E_2 with fiber volume fraction

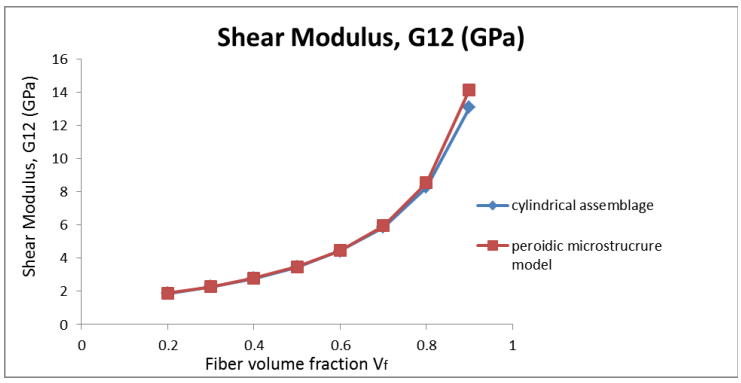

Figure 5. Variation of $G_{12}$with fiber volume fraction.

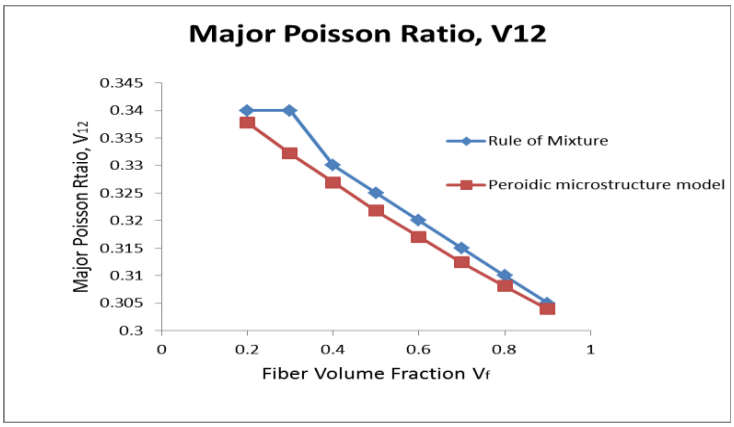

Figure 6. Variation of V_{12} with fiber volume fraction.

(R- Glass / Epoxy lamina)

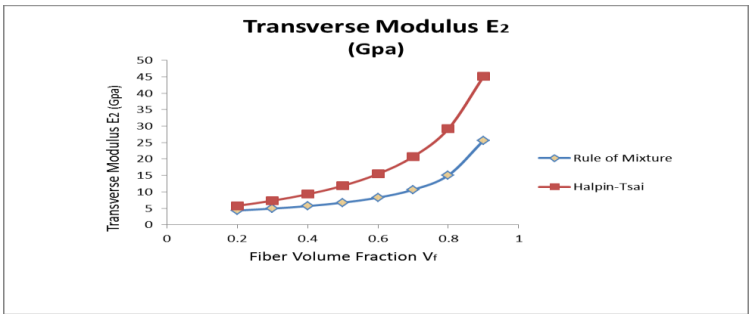

Figure 7. Variation of E_2 with fiber volume fraction

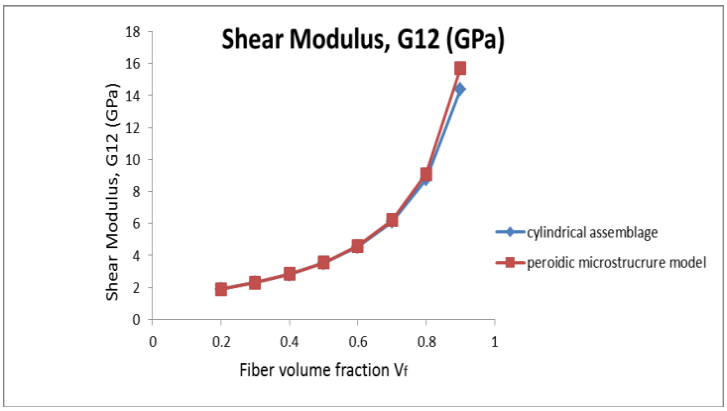

Figure 8. Variation of $G_{12}$with fiber volume fraction.

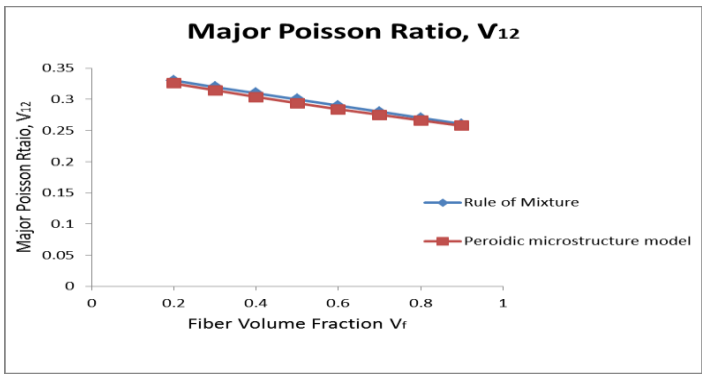

Figure 9. Variation of V_{12} with fiber volume fraction.

(S- Glass / Epoxy lamina)

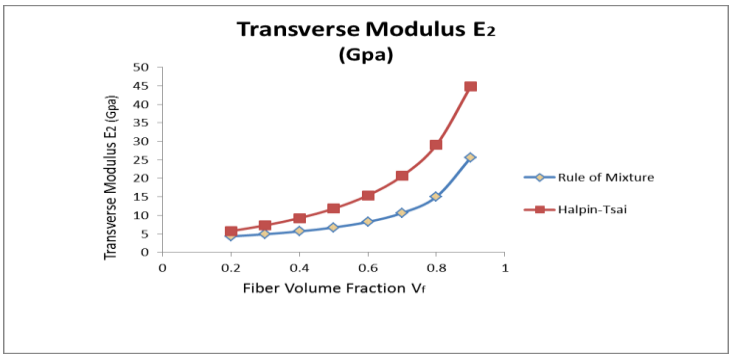

Figure 10. Variation of E_2 with fiber volume fraction

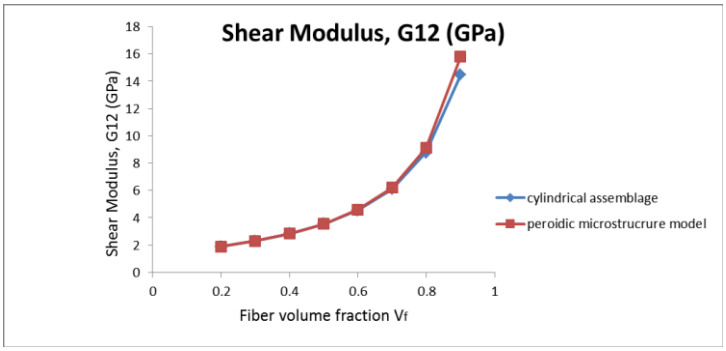

Figure 11. Variation of $G_{12}$with fiber volume fraction.

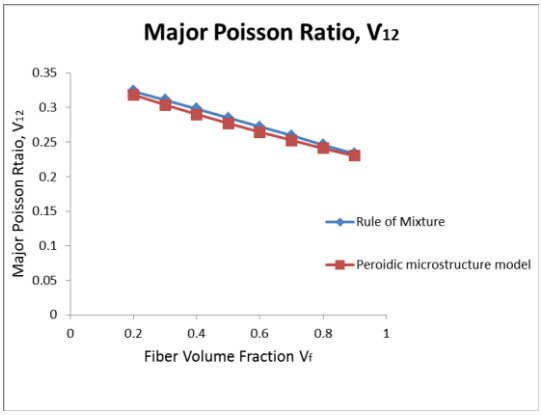

Figure 12. Variation of V_{12} with fiber volume fraction.

- For all composites, Poisson's ratio V_{12} is decreasing with increasing the fiber volume fraction. However, for E-Glass/Epoxy, the magnitude of V_{12} computed by ROM tries to stay at same level at the beginning of the curve, but rapid decrease happens after that making noticeable difference with the magnitude of this computed by PMM.
- Generally, it can be seen that the longitudinal modulus E1 is increasing with the increase of fiber volume fraction. Also, there is a linear increment of the transverse modulus E_2 with the increment of fiber volume fraction. In addition, in plane Shear modulus G_{12} increases linearly with increase in fiber volume fraction for all the three types of glass fibers. However, for all composites, Poisson's ratio V_{12} is decreasing with increasing the fiber volume fraction.

2.3 Experimental Modal Analysis for an Artificaiily Damaged Composite Component

This experiment presents the investigation of the Noise, Vibration and Harshness (NVH) behaviour of damaged and not damaged fiber reinforced polymer FRP test probes with simple geometry. For that purpose, artificial defect/failure generation procedure for the test probes will be developed and applied. Afterwards some NVH measures, e.g., natural frequencies, modal damping and mode shapes will be evaluated. The results will show on the one hand the sensitivity of the measurement method for damages and on the other hand the change of the NVH characteristics of the probes through damages.

One of the test methods, which can describe the NVH characteristics of a structure, is the modal analysis. The method delivers the modal frequencies, mode shapes and modal damping where the parameters can be more or less responsible for the NVH behaviour of a vehicle. If the excitation meets a modal frequency, and the mode shape at that modal frequency has good radiation efficiency or the path of vibration transfer from that part to another in the vehicle is sufficient, this method will be applied for the investigations. After getting the results of the modal test, they will be analyzed, and the change of the modal behaviour between undamaged and damaged specimen will be explained. At the end the eligibility, respectively the sensitivity of the modal analysis method for crack detection at FRP should be verified.

2.3.1 The Test Specimen

For the further investigations we selected a glass reinforced plastic plate with the material type of MF GC 201 (melamine resin laminate) due to the simple accessibility, and similar types are often used by vehicles. The specimen had a simple rectangular shape with the dimensions of (500x200x3 mm). Two Artificial damages are made in the specimen by an air gun. The first is barely seen as a result of the impact of the small buckle of the gun. The second damage is a crack with a length of 70 mm (figure 13). So, we used that cracked specimen for the further investigations. Overall 30 measurement points are defined on the plate, to be able to represent the mode shapes, which tend to have more local displacement, than global.

This number of points should be sufficient enough for that. Measurement point No. 30 is also acted as the excitation point.

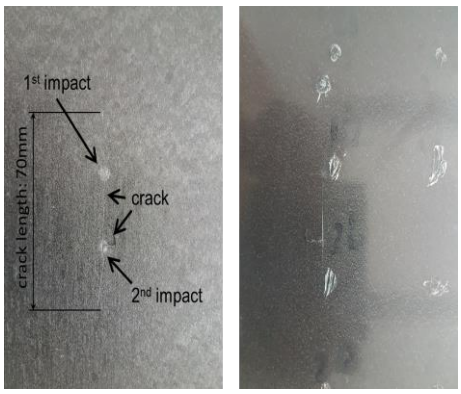

Figure 13. Damage of the Specimen (left: side of the impact; right: back side).

2.3.2 Results

Looking at the individual resonances (roughly 20 pieces up to 500 Hz) in the range from 110 to 190 Hz (Figure 14), differences in level of the peaks, and missing resp. new peaks can be found in the averaged FRF of the cracked plate compared to the un-cracked one.

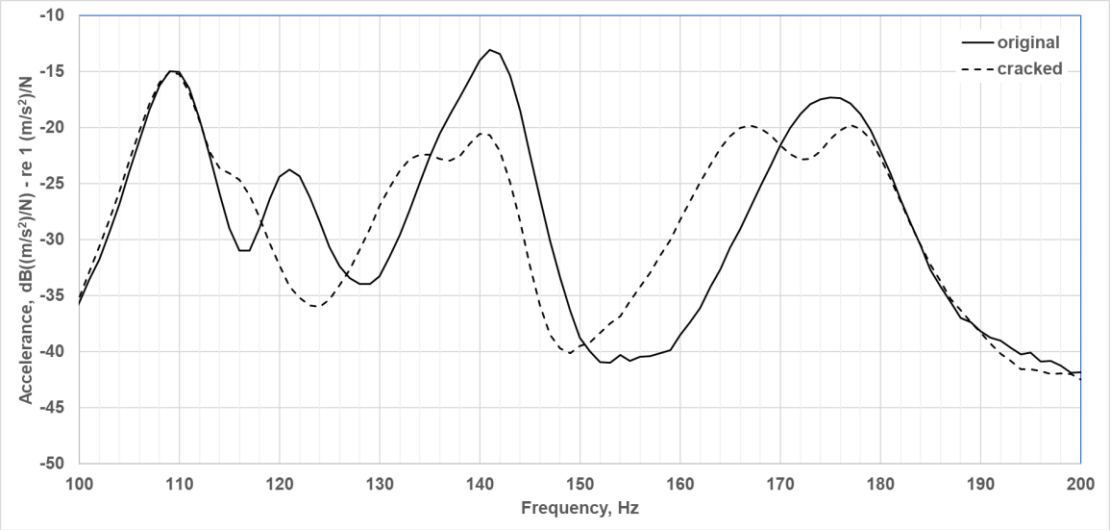

Figure 14. The Average of the Measured FRFs for the Uncracked and for the Cracked Specimen (from 100 to 200 Hz).

It can be stated that an existing crack in the material causes the appear and the disappear of certain resonances. Presumably the modes are not appearing/disappearing, they are always there, but due to the crack they will be simply better or worse excited, depending on the frequency, mode shape and damping. By performing the complete modal analysis, the assumption before could be boosted. That means the resonance peaks changing (appearing or disappearing) significantly, where a large relative displacement between the measurement points in the surrounding of the crack of a mode shape can be observed. On our cracked

specimen the crack is ranging approximately from the measurement point 14 to 20, and here also a large displacement can be observed.

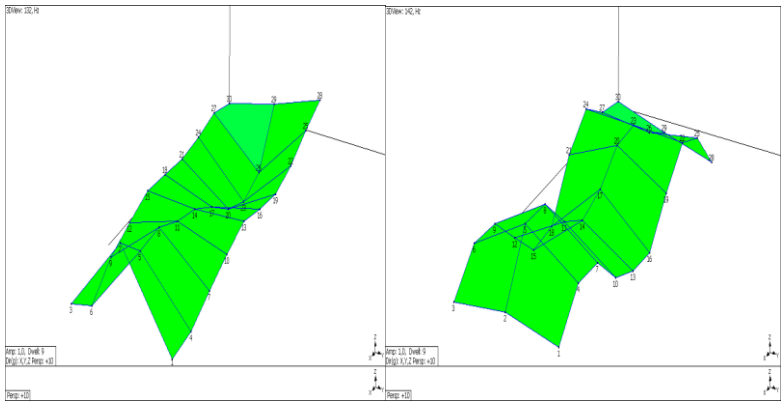

Figure 15. Two Mode Shapes of the Cracked Plate by 132 Hz (left) and 142 Hz (right), Displacement in the Z direction.

2.4 Damage Detection in a Fibre Reinforced Polymer Component by the Vibration Decay Rate and the Damping Behaviour

Considering that the damages of composite materials have an effect on the vibration decay rate, this chapter includes using the experimental measured decay rate to predict the damage presence on the specimen. The measured decay rate shows an estimation of the dynamic behaviour of the target part. The focus of the current investigation is to do laboratory work for measuring the vibration decay rate of a FRP composite component [10].

In addition to that, Current chapter investigates the damping response offered by a damaged fiber reinforced polymer plate. The plate is put under three different conditions regarding the damage existence. The focus is to measure the loss factor in all cases and determine whether there is difference among them to prove damage presence in the composite part. The loss factor is experimentally measured by measuring the vibration decay time RT60. The resulted data of loss factor show a well distinguished difference that might lead to predict damages, and to do more expanded analysis of this issue. The loss factor which is obtained through the measurement of the decay time RT60 is measured for the three cases of the plate. The obtained data of each one is investigated individually and compared with each other attempting to conclude an overview of damages presence in the tested component.

The composite material specimen undergoes three different states based on the damage existence in it. In each state, the decay rate is done and the result data is measured. Distinguish the difference in the response of the dynamic behaviour in each case is analysed and considered to indicate the damage existence.

The filtered RT60 is related to loss factor over the frequency by the following formula [11]:

$$\eta(f) = 2.2 / f._{RT60} \quad (12)$$

where

f: is the mid frequency of a third octave band in Hz.

RT_{60}: is the decay rate for each third octave mid frequency in s.

The value of *2,2* is derived from the energy drop to the one millionth of the initial value.

2.4.1 The Test Specimen

For the investigations, a material type of MF GC 201 (melamine resin laminate) is selected. It is a glass reinforced polymer that consists of several layers of glass cloth impregnated with melamine. The specimen has a simple rectangular shape with the dimensions of (500 x 200 x 3 mm), as shown in figure 16. The material tensile strength is 150 MPa while the compressive strength is 275 MPa. The modulus of elasticity of the material is 1400 MPa.

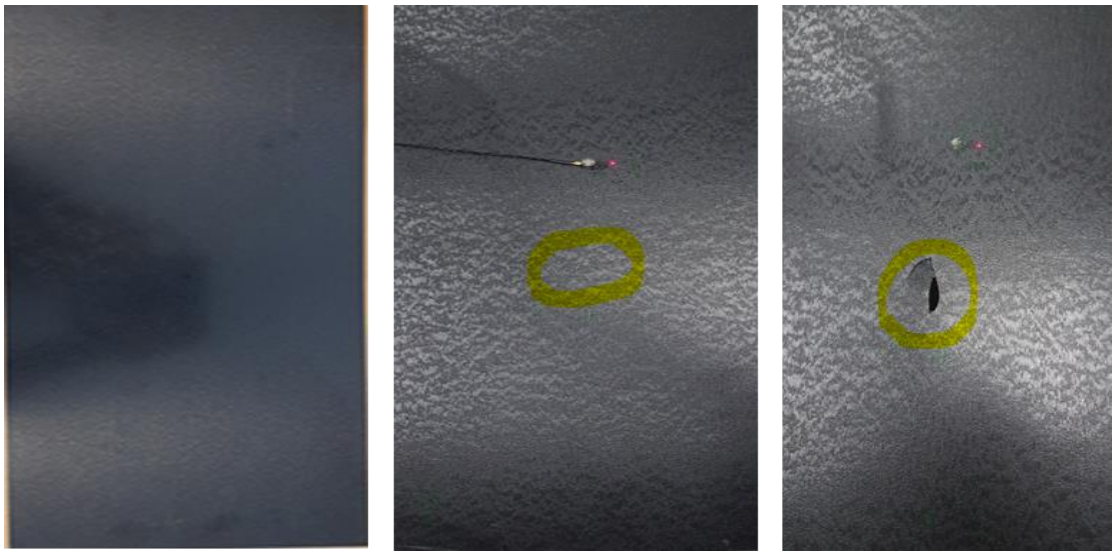

Figure 16. The Test Specimen with Three conditions.

2.4.2 Performing the Test

Three excitation points and one measurement point were determined to perform the hits and record the results. The first excitation points is the middle of the specimen, while the second and third were (10, 10) and (3, 5) from the lower edge respectively. The measurement point is horizontally in the middle and vertically in the upper one-third of the part. As mentioned; the test is done three times according to the three different conditions of the specimen. First time, the specimen is free of damages while the second time the specimen is damaged, but the crack is barely seen by eye supposing that there are damages in the microstructure of the part which may be detected by the resulting signal. The third test is done when the specimen is fully cracked as there is a gap in the spacemen. During each time of the test, the excitation points are respectively hit ten times by the hammer and the recorded data

were averaged. All recorded data are analysed by the Room Acoustic Wizard software and graphs are generated.

2.4.3 Analysis of the Vibration Decay Rate Results

The graph in figure (17) shows the RT60 of all three states together. As it is clear in the figure, after 1000 Hz, there is a big difference can be seen among the three of them.

The damaged condition no.2 (grey line) showing the highest RT60 conflicting the fact that a part of the material (a fragment) is missing, so the internal material damping is less.

Same fact can be applied to the damaged case no.1 (orange line) considering that there is a crack so there is micro-displacement between the crack surfaces (Coulomb-friction), so the damping is increased compared to the original specimen.

In accordance with the results above, the presence of damages can be estimated by the vibration decay rate in specific condition.

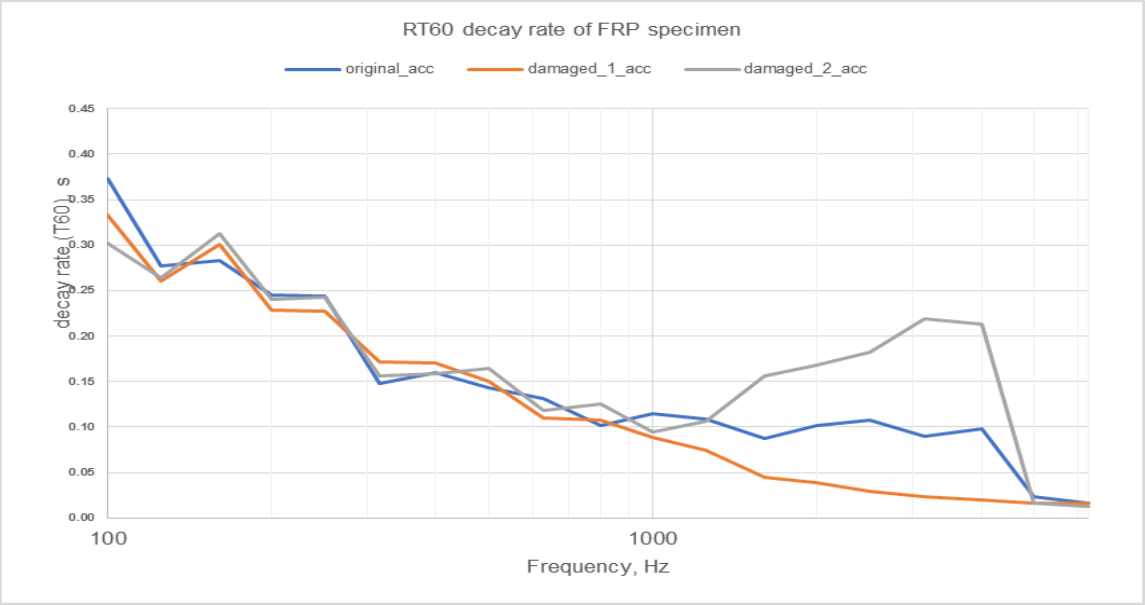

Figure 17. RT60 Decay Rate of the Three Cases.

2.4.4 Analysis of the Loss Factor Results

Figure (18) shows the relation of the loss factors for the three different damage conditions of the same specimen. Up to 1000 Hz there is no difference in damping behaviour. Beyond 1000 Hz significant differences of the loss factors can be observed. The loss factor of the damaged-1 specimen is three times higher as that of the original. The damage-1 condition means only a barely visible crack in the plate, so that micro-sliding occurs. This is producing the Coulomb-friction between the cracked surfaces, which is finally dissipating the vibration energy faster than in the original condition. In case of damaged-2, material area of (0.5 x 2 cm) is cracked out from the specimen, so this area fragment is practically missing. In this case, over 1000 Hz, the loss factor is roughly half as high as in original condition. Due to the

missing material fragment the Coulomb-friction cannot take effect, so the loss factor is reduced. In addition, the missing material fragment means also less internal damping generating micro-mechanisms, with the result of less damping than the original. It is quite surprising, that so small missing part causes a significant drop of the loss factor.

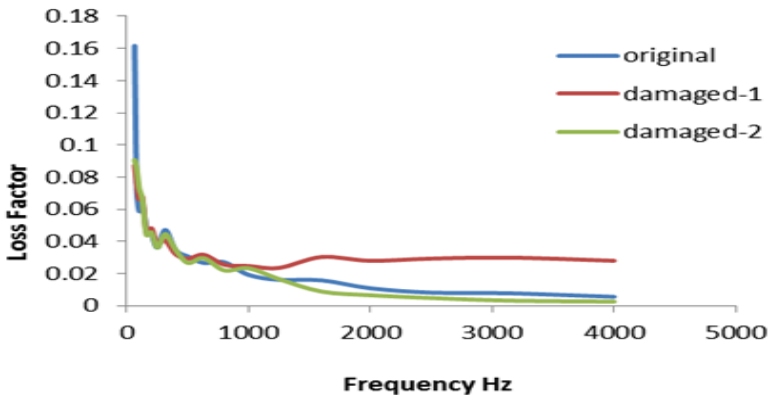

Figure 18. The Loss Factor of the Three Cases.

2.5 Modal analysis of Pre-Tensile-Loaded composite plates

The goal of the investigation was to determine the modal behaviour of the specimen with different preload condition, resp. with different material damage condition resulting from the tensile loading. Two specimens with different geometry were used for the tests. The first one was a probe with 250x25x3 mm dimensions, the second was slightly different, with the same surface area but with 5 mm thickness. The specimen was put into a tensile pull machine and was loaded with different loads. The 3 mm thick probes were loaded with forces, which caused 2 mm, 4 mm and 6 mm length extension. The 4th probe was kept unloaded; it served as the reference probe. Similar to that the 5 mm thick probes were also loaded, with 2,5 mm, 5 mm and 7,5 mm length extension of the probes. The 4th was kept unloaded. After loading the probes, the force was released, so the probes could take their unloaded length. The goal of the tensile loads was to create damages inside material structure of the probes.

2.5.1 The Test Specimen

Two composite plates of (250x25x5) mm and (250x25x3) mm were used in this test. The plates are made of glass fiber reinforcing epoxy resin. The specimens were provided by Quattroplast Hungary Company.

2.5.2 Measurement setup

The probes were put onto a TIRA TV 50009 electrodynamic vibration test system (shaker) as shown in figure 13. The shaker can provide a 9 N excitation force as maximum. The probes were mounted sequentially on the shaker interconnected with a PCB 288D01 impedance head.

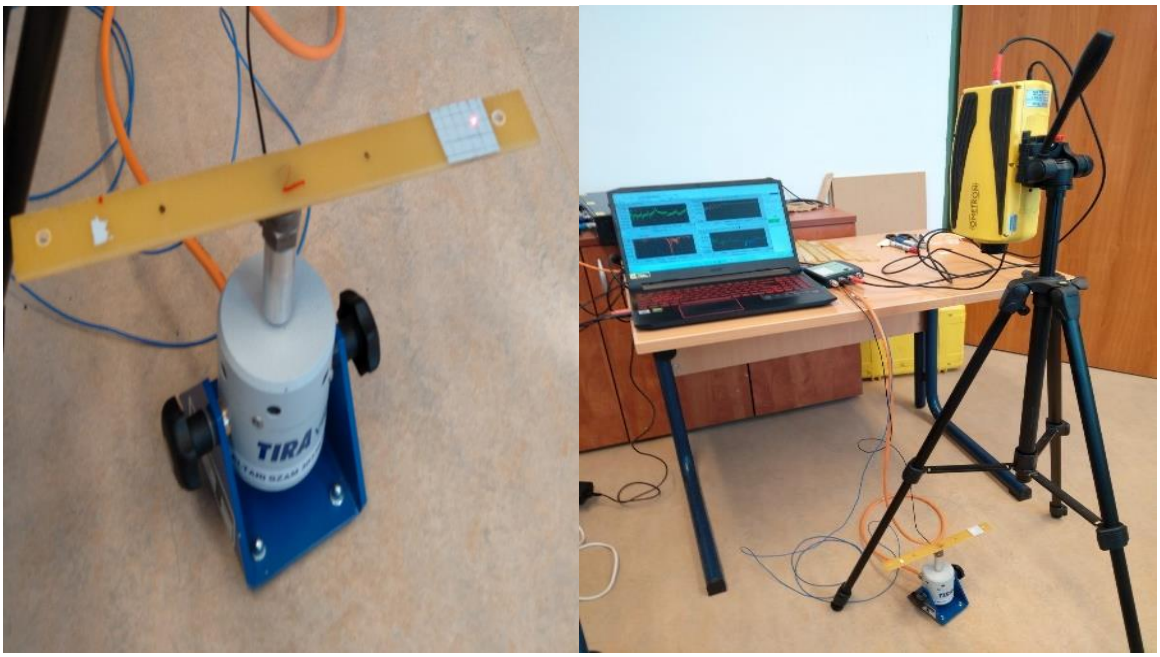

Figure 19. The Test Set Up.

The probes were put onto a TIRA TV 50009 electrodynamic vibration test system (shaker) as shown in figure 8.1. The shaker can provide a 9 N excitation force as maximum. The probes were mounted sequentially on the shaker interconnected with a PCB 288D01 impedance head. The probes were glued on the mounting plate of the impedance head with HBM X60 two components cold curing glue at the half length of the probes. With the impedance head the exciting force and the vibrational acceleration at the exciting point could be measured. Roughly 90 mm from the middle of the probe (only one side) a reflective patch was fixed on the probe surface. At this point the vibration of the probe due to the excitation was measured with an out of plane laser doppler vibrometer Ometron VH-1000 (B&K 8338).

The measured signals (force, acceleration, velocity) were connected to a 4 channel DAQ (B&K Photon +). The measurement software created the desired functions, in this case the frequency response functions (FRF) between force and acceleration ($m/s^2/N$) and force and velocity (m/s/N), the coherences for each FRFs. The FRF acceleration over force (a/F) is called inertance, the velocity over force (v/F) is called mobility.

2.5.3 The results

The FRF functions, inertance and mobility were represented in diagrams for each probe (figure 20). The curves are showing the resonance frequencies of the probes. Additionally, a FEM model of the probe was created and FEM calculations were performed in order to determine the mode shapes for each resonance frequency. (Performing the FEM calculation was easier and faster than to perform a measurement, since for the measurement roughly 40 points had to be measured sequentially on the probe to represent the probe geometry with a proper accuracy.)

The FRRs are showing that the resonance frequencies of the unloaded probe have higher frequency resonances than the loaded ones. The differences in frequencies for each resonance (for unloaded and max. loaded (7,5 mm) probe) are the following:

Table 2. Differences of the Resonance Frequencies of the Unloaded and Max. Loaded Probe of (5mm Thickness)

Nr.	**Un-loaded probe**	**Max. loaded probe**	**difference**
1.	323 Hz	311 Hz	12 Hz
2.	1635 Hz	1615 Hz	23 Hz
3.	4054 Hz	3910 Hz	144 Hz
4.	7525 Hz	7128 Hz	398 Hz
5.	11466 Hz	10938 Hz	528 Hz
6.	15915 Hz	15280 Hz	635 Hz

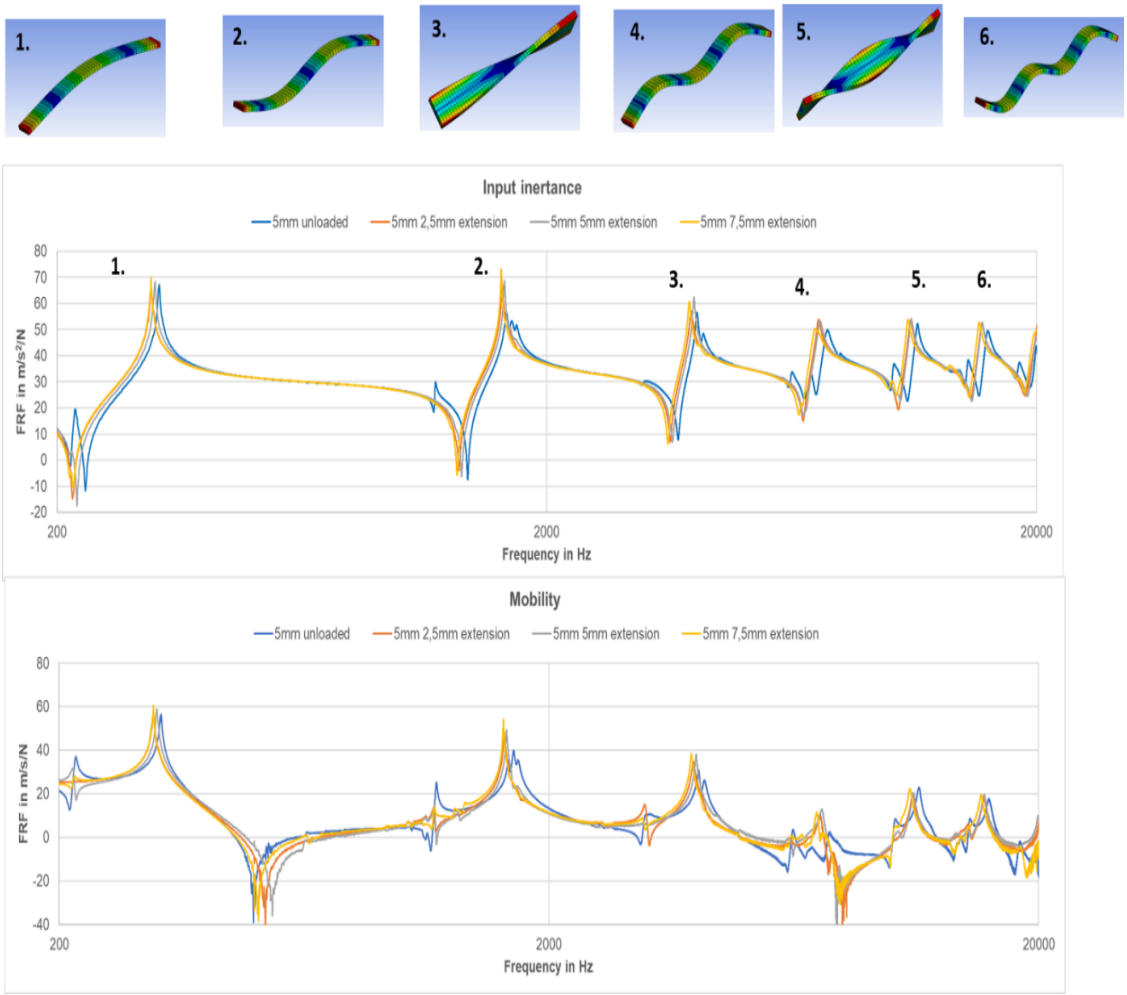

Figure 20. The Resonance Frequencies of the First Specimen (5mm thick).

As shown in figure 20, the damage of the probe material due to external loading through a tensile test machine has a significant effect on the resonance frequencies of the probes. It means that the probes behave less stiff as in unloaded condition. This behaviour can be explained through the damage of the matrix or the glass fiber. Which of them, resp. in which dimension is responsible for the stiffness falling can only be explained with CT tests which is shown in the next section.

Going upwards in the frequency axis the mode shapes became more and more complex. The global modes (e.g., the first bending mode) are less affected; the more complex modes are more affected from the internal material damage. The above-described behaviour also can be noticed for the probes with less extension (2,5 mm and 5 mm), of course with less difference in the resonance frequencies.

2.5.4 The C-T Scan Results

Figure 21 shows some CT scan views of the specimen. In order to figure out the change in the microstructure, the focus was on the woven fabric in the front view.

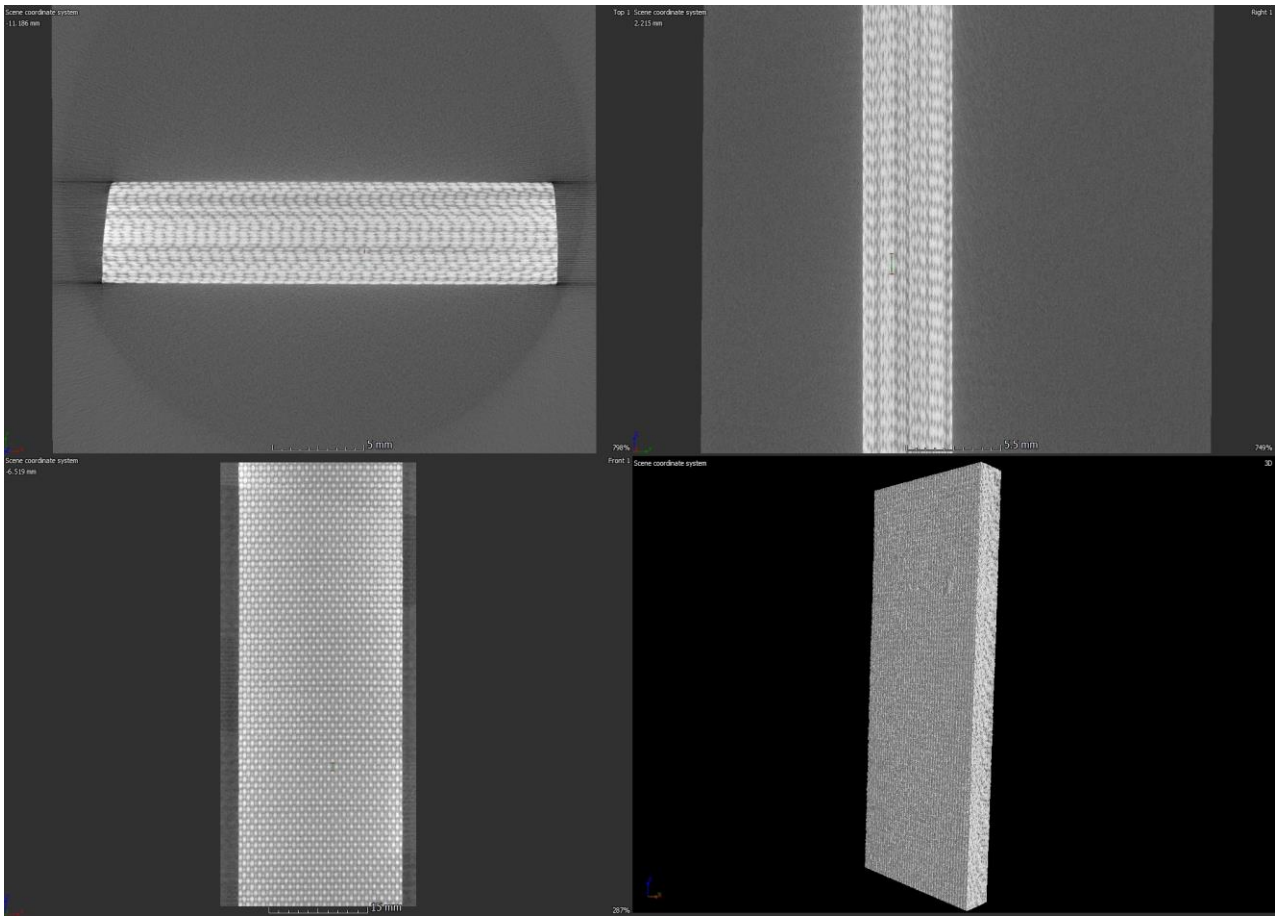

Figure 21. CT Scanning Views of the Specimen

At First sight, it is not clear that there is flaw or defect in the material constituents between the unloaded and the loaded cases of the specimen. Thus, to investigate more deeply, Distances between every two points of the woven fabric of the unloaded and the maximum

loaded specimen are measured. The results show that approximately the distances between the points in the woven fiber of the microstructure image in the unloaded case is 1.004 mm while in the max loaded case is 1.57 mm as it shown in figure 22.

This could be also an indication of the damage effect because there is a different displacement between the measured points of two specimens. It might be an indication of beginning of damage such as fiber matrix debonding or delamination.

Although there is very slight displacement between the woven fibers, it is clear that the modal analysis method is more sensitive to detect such damages

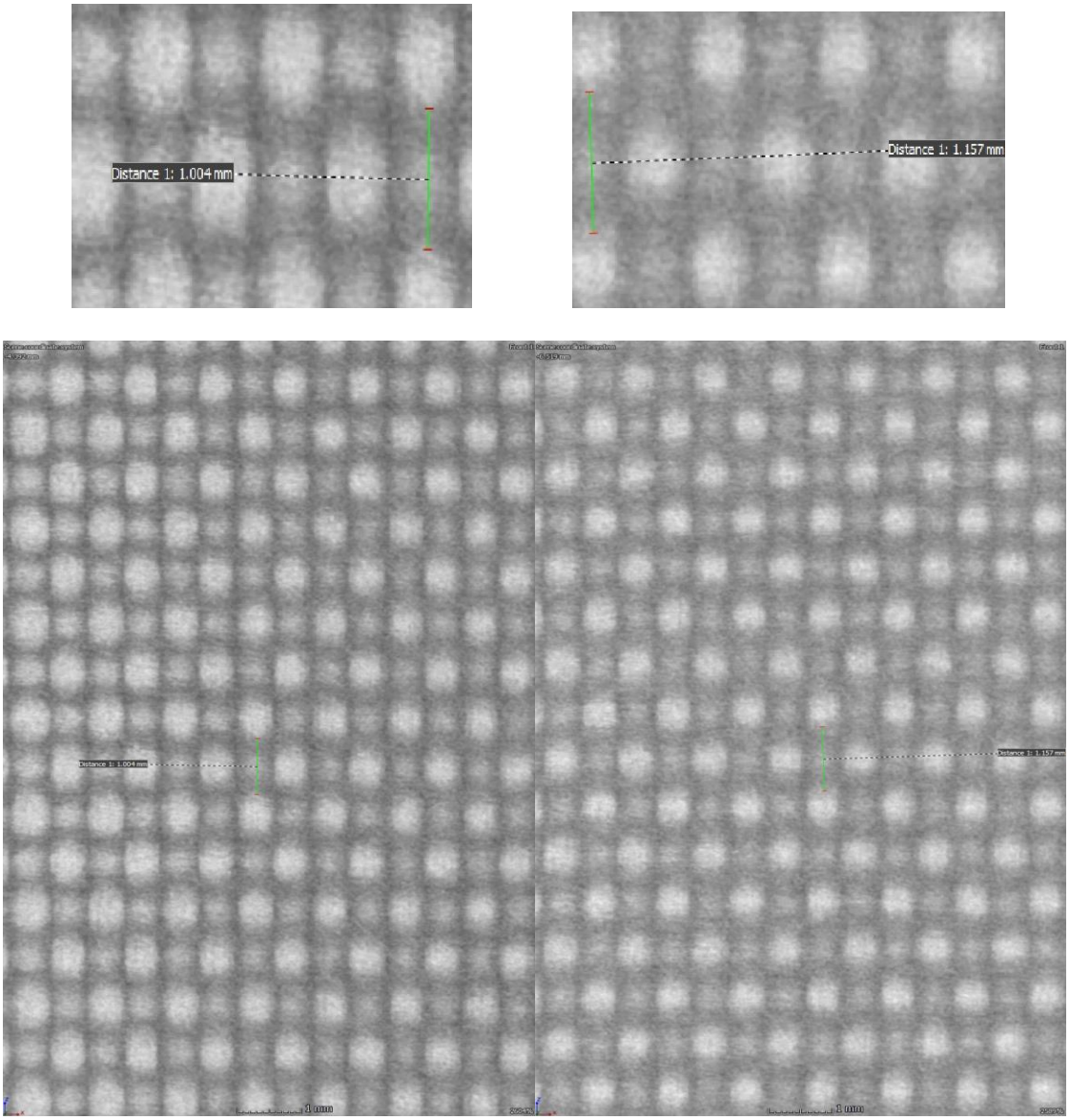

Figure 22. Distance Between the Tow Points of the Woven Fiber in the Specimens (left un loaded), (right: the max.loaded).

3 NEW SCIENTIFIC RESULTS – THESES

T1. I used particle swarm optimization (PSO) to find the best design parameters including spatial elements of the unit cell as well as a given set of strength values for both Glass-fiber and Epoxy. A comparative study is done to select optimal fibre diameter that can satisfy the optimal longitudinal tensile strength. Thus, I proved that PSO was efficient enough to find the best possible design parameters within only five iterations [K2].

T2. I used the micromechanical theories to prove that the longitudinal modulus E_1 is increasing with the increase of fiber volume fraction. Also, there is a linear increment of the transverse modulus E_2 with the increment of fiber volume fraction. In addition, in plane Shear modulus G_{12} increases linearly with increase in fiber volume fraction for all the three types of glass fibers. However, for all composites, Poisson's ratio ν_{12} is decreasing with increasing the fiber volume fraction. The investigation is done on three types of glass fibers reinforced polymer lamina [K5].

T3. I investigated the noise, vibration, and harshness (NVH) behavior of damaged and not damaged fiber reinforced polymer FRP plate by using the modal analysis method. The results that we found showed that the modal analysis is an effective tool for detecting such damages because it is clearly observed that the method is sensitive of to the damage existence. Also, it is indicated that there are changes in the NVH characteristics of the specimens due to the damages [K1].

T4. I experimentally used the vibration decay rate as a method to detect damages in a FRP component. Measurement of reverberation time RT60 is executed in three different damage conditions of a specimen made of fibre reinforced polymer. I proved that the method is able to estimate the presence of damages in the part as the measured RT60 showed a clear difference after 1000 Hz of frequency between all three cases (undamaged / damaged 1/ damaged 2) specimens [K4] .

T5. I investigated the damping response offered by a damaged Fiber-reinforced polymer plate. The plate is is elastically supported and put under three different conditions regarding the damage existence. I found that the loss factor of the damaged-1 specimen is three times higher than that of the original. In case of damaged-2, over 1000 Hz, the loss factor is roughly half as high as in the original condition. In my investigation, I found that the damping behavior of the composite specimen gives clear indication about the damage status of the material [K6].

T6. I studied the modal behavior of glass fiber reinforced epoxy specimen with different pre tensile-loaded conditions. The results I found show that the damage of the probe material due to external tensile loading has a significant effect on the resonance frequencies of the probes. I proved, that the probes behave less stiff as in unloaded condition. This behavior can be explained as that the load has caused damage in the matrix or in the reinforcement part or in both.

4 LIST OF PUBLICATIONS RELATED TO THE TOPIC OF THE RESEARCH FIELD

K1. Alsarayefi, S. J., and K. Jalics. "The change of the NVH characteristics of composite vehicle components as a result of visible and not visible damages." In *Advances and Trends in Engineering Sciences and Technologies III: Proceedings of the 3rd International Conference on Engineering Sciences and Technologies (ESaT 2018), September 12-14, 2018, High Tatras Mountains, Tatranské Matliare, Slovak Republic*, p. 9. CRC Press, 2019.

K2. Alsarayefi, Saad, Hazim Nasir Gafil, and Károly Jálics. "Optimization of the fiber size for a fiber glass epoxy composite." *Design of Machines and Structures* 9, no. 1 (2019): 5-12.

K3. Saad, Alsarayefi, and Károly Jálics. "Application of Experimental Modal Analysis to Investigate Damage to Fiber Reinforced Composites." *Multidisciplinary Sciences* 9, no. 4 (2019): 275-282.

K4. Alsarayefi, Saad, and Károly Jálics. "Damage Detection in a Fiber Reinforced Polymer Component by the Vibration Decay Rate." *JOURNAL OF ADVANCED RESEARCH IN DYNAMICAL AND CONTROL SYSTEMS* 12, no. SP8 (2020): 644-650.

K5. Alsarayefi, Saad, and Károly Jálics. "Micromechanical Analysis of Glass Fiber/Epoxy Lamina." In *Vehicle and Automotive Engineering*, pp. 101-111. Springer, Singapore, 2020.

K6. Alsarayefi, S., and K. Jalics. "Anticipation of damage presence in a fiber reinforced polymer plate through damping behavior." *Engineering Solid Mechanics* 9, no. 3 (2021): 263-270.

K7. Saad, Alsarayefi, and Jálics Károly. "Kísérleti modális elemzés alkalmazása szálerősítéses kompozitok károsodásának vizsgálatához." *Multidiszciplináris Tudományok* 9, no. 4 (2019): 275-282.

5 LITERATURE CITED IN THE THESES BOOKLET

1. Rajak DK, Pagar DD, Menezes PL, Linul E (2019) Fiber-reinforced polymer composites: Manufacturing, properties, and applications. Polymers (Basel) 11:1667. https://doi.org/10.3390/polym11101667
2. Günaslan SE, Karaşin A, Öncü ME (2014) Properties of FRP materials for strengthening. Int J Innov Sci Eng Technol. 1(9):656-60
3. Jollivet T, Peyrac C, Lefebvre F (2013) Damage of composite materials. In: Procedia Engineering. 66:746-58
4. Razali N, Sultan MTH, Mustapha F, et al (2014) Impact Damage on Composite Structures – A Review. Int J Eng Sci3(7):08-20.
5. Heslehurst RB (2014) Defects and Damage in Composite Materials and Structures. CRC press, Boca Raton, FL, USA.
6. Gholizadeh S (2016) A review of non-destructive testing methods of composite materials. In: Procedia Structural Integrity. Elsevier B.V., pp 50–57
7. Alberto M (2013) Introduction of Fibre-Reinforced Polymers − Polymers and Composites: Concepts, Properties and Processes. In: Fiber Reinforced Polymers - The Technology Applied for Concrete Repair
8. Melro AR, Camanho PP, Andrade Pires FM, Pinho ST (2013) Micromechanical analysis of polymer composites reinforced by unidirectional fibres: Part I-Constitutive modelling. Int J Solids Struct 50:1897–1905. https://doi.org/10.1016/j.ijsolstr.2013.02.009
9. Kashtalyan M (2018) Introduction to Composite Materials Design– Third editionE. J. Barbero CRC Press, Taylor & Francis Group, 6000 Broken Sound Parkway NW, Suite 300, Boca Raton, FL, 33487-2742, USA. 2018. Distributed by Taylor & Francis Group, 2 Park Square, Milton Park, Ab. Aeronaut J. https://doi.org/10.1017/aer.2018.135
10. Chen YM, Liu QX, Liu JK (2019) Time-Dependent Decay Rate and Frequency for Free Vibration of Fractional Oscillator. J Appl Mech Trans ASME. 86(2):024501 https://doi.org/10.1115/1.4041824
11. Fahy F (2003) Foundations of Engineering Acoustics. Elsevier